2026 NDIA MICHIGAN CHAPTER
GROUND VEHICLE SYSTEMS ENGINEERING
AND TECHNOLOGY SYMPOSIUM
MODELING, SIMULATION, PROTOTYPING, AND VALIDATION (MSPV) TECHNICAL SESSION
AUGUST 11-13, 2026 - NOVI, MICHIGAN

ATOMISTIC MOLECULAR DYNAMICS STUDY OF LINEAR AND BRANCHED IMIDAZOLE-FUNCTIONALIZED POLYMERS

Sujith Ganta[1], Twaha Alim[1], Leela Rakesh, PhD[1], Anja Mueller, PhD[1], Axel Mellinger, PhD[1], Theodore Burye, PhD[2], Talia Sebastian, PhD[2]

[1]Central Michigan University, Mt. Pleasant, MI
[2]US Army DEVCOM GVSC

ABSTRACT

We present atomistic molecular dynamics simulations of linear and branched fluorinated polymer chains, with and without imidazole functionalization, designed as a model for solvent-free proton-conducting membranes for high-temperature fuel cell applications. Simulations conducted over a temperature range of 300 to 550 K, and diffusion-based relaxation times reveal that glass transition temperatures depend on polymer architecture: the branched and functionalized systems exhibit transitions near 400 K compared to 500 K for the linear chain. Fluorine-fluorine radial distribution functions demonstrate that branching disrupts local packing order, while imidazole substitution creates specific intra-chain interactions. Radius-of-gyration distributions reveal that branching significantly increases chain extension and creates multiple conformational families, whereas imidazole groups stabilize compact conformations at low temperatures that transition to more diverse states upon heating. These findings provide molecular-scale insight into how polymer architecture controls thermal transitions and structural organization in model high-temperature polymer electrolyte membranes.

Citation: S. Ganta, T. Alim, L. Rakesh, T. Burye, A. Mueller, A. Mellinger, T. Sebastian, "Atomistic Molecular Dynamics Study of Linear and Branched Imidazole-Functionalized Polymers," In Proceedings of the Ground Vehicle Systems Engineering and Technology Symposium (GVSETS), NDIA, Novi, MI, Aug. 11-13, 2026.

1. INTRODUCTION

Proton-exchange membrane fuel cells (PEMFCs) are promising energy conversion devices due to their high efficiency, low emissions, and potential for both stationery and transportation applications, including ground vehicle power systems [1]. The performance and durability of PEMFCs are critically governed by the polymer electrolyte membrane, which must combine high proton conductivity with mechanical robustness and chemical stability over extended operation at elevated temperatures [2-4]. Conventional perfluorosulfonic acid membranes rely on water to sustain proton transport [5], limiting operation to relatively low temperatures and

introducing challenges associated with water management in vehicle applications [3,6].

One strategy for achieving high-temperature proton conduction is to introduce basic functional groups, such as imidazole or related heterocycles, into the polymer architecture [7-8]. These groups can form extended hydrogen-bond networks that support Grotthuss-type proton hopping even in the absence of bulk water [9]. At the same time, polymer backbone design and degree of branching influence structural properties, which impact transport properties and mechanical behavior. Understanding how these architectural parameters affect proton mobility and local structure is therefore essential for rational membrane design.

Atomistic molecular dynamics (MD) simulations are widely used to compute temperature- dependent diffusion coeffi-cients and to analyze structural descriptors in polymer and polymer-electrolyte systems [9]. These simulations provide molecular-level information on transport and local structure [9-13]. Furthermore, by varying chain length, topology, or functional group patterning, MD can isolate the influence of individual architectural parameters on the structure in a controlled manner [4,11-14].

In this work we are investigating three fluorinated model polymer architectures relevant to solvent-free, high-temperature proton-conducting membranes for vehicle power applications. The set includes an 8-unit linear chain (8L), an 8-unit chain with four branches (8L4B), and an 8-unit branched chain with imidazole functionalization (8L4B-4Iz). These systems are chosen to systematically vary branching density and functionalization while keeping the underlying chemical motif and chain length similar. We focus on three main questions: (i) how apparent glass transition temperature, inferred from diffusion behavior, depends on architecture; (ii) how radial distribution functions (RDFs) capture changes in local packing and structural order; and (iii) how radius-of-gyration (R_g) distributions reveal conformational "phases" and their evolution with temperature.

The simulations show clear signatures of glass-like to liquid-like transitions in diffusion data, strong dependence of local order on chain architecture, and rich conformational behavior associated with branching and imidazole substitution. Together, these results build a coherent molecular-level story that can guide the design of high-temperature polymer electrolyte membranes for ground vehicle fuel cell systems.

2. METHODS

2.1. Polymer Systems

Three polymer architectures were constructed based on the same monomer structure (Figure 1) to systematically investigate the effects of the polymer backbone, branching, and imidazole functionalization**:**

- 8L: An 8-repeat-unit fully linear chain without branches or imidazole groups
- 8L4B: An 8-unit chain with four short branches, representing a moderately branched architecture

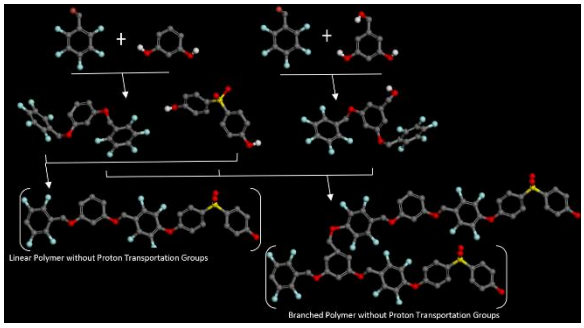

Figure 1: Schematic of the polymerization reaction from monomer to linear and branched polymers

- 8L4B-4Iz: An 8-unit chain with four branches, where selected sites are functionalized with imidazole groups

These systems serve as model structures for simulation purposes of fluoroaromatic polymers. The analysis presented here emphasizes generic features of polymer architecture rather than specific chemical reactions or proton transfer events. Notably, these architectures and modifications are also being synthesized and studied experimentally, ensuring that the simulations reflect realistic laboratory conditions.

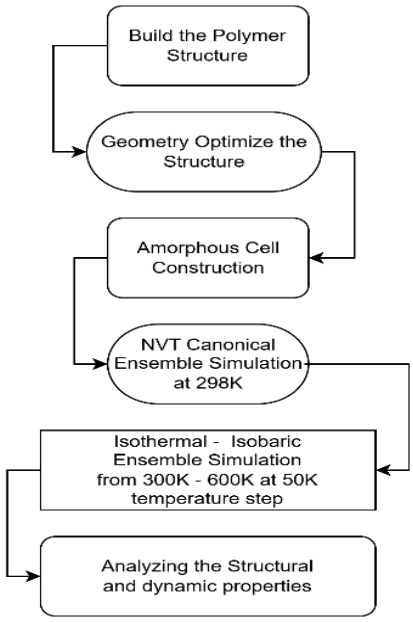

Figure 2: MD simulation workflow in BIOVIA Materials Studio [15], showing system construction, optimization, equilibration, production run, and analysis of structural properties.

2.2. Simulation Setup

All molecular dynamics (MD) simulations in this study were performed using Materials Studio 6.0 (BIOVIA, San Diego, CA), with the COMPASS (Condensed-phase Optimized Molecular Potentials for Atomistic Simulation Studies) force field applied consistently throughout via the Amorphous Cell and Forcite Plus modules. COMPASS is a well-established *ab initio*-derived force field that covers a wide range of elements and valence states, which makes it a natural fit for the chemically diverse systems studied in this paper [16-17].

The Forcite Plus engine integrates Newton's equations of motion using the Verlet leapfrog algorithm [18]; long-range electrostatic interactions are handled through Ewald summation, while van der Waals interactions are truncated with an atom-based cutoff and tail corrections applied beyond it. Temperature and pressure were held stable using the Nose-Hoover thermostat and Berendsen barostat throughout both equilibration and production. The Amorphous Cell module built the initial bulk polymer configurations through a Monte Carlo chain-growth procedure that respects excluded-volume constraints during packing.

Polymer chains were constructed in three architectures - linear (8L), branched (8L4B), and branched imidazole-functionalized (8L4B-4Iz) - following the designed repeat-unit structures, with the full simulation workflow shown in Figure 2. Each single-

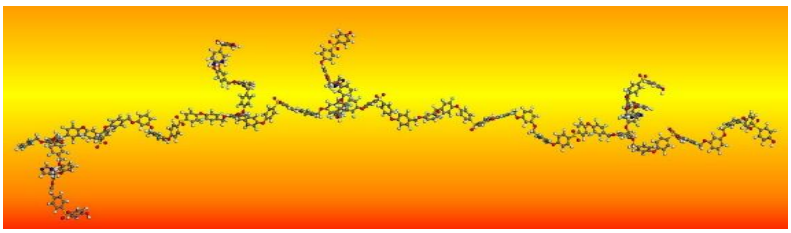

Figure 3a: Molecular structure of the unoptimized 8L4B-4Iz polymer.

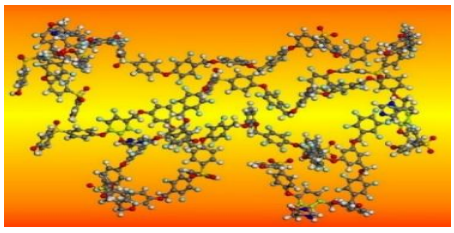

Figure 3b: Optimized structure of the 8L4B-4Imz polymer.

chain model (Figure 3a) was first geometrically optimized to remove any strained contacts, then equilibrated in the NVT ensemble at 300 K for 5 ns. The lowest-energy configuration from this stage (Figure 3b) was carried forward into the bulk modeling.

That optimized chain was then packed into a three-dimensional cubic cell under periodic boundary conditions using the Amorphous Cell module, with a target nanocomposite density of 1.2 g/cm³. The resulting amorphous cell (Figure 4) was geometrically optimized using the Smart algorithm - which works sequentially through steepest-descent, conjugate gradient, and Newton-Raphson steps - running for at least 1×10^5 steps until a well-converged minimum was reached. From there, equilibration proceeded in two stages: a 5 ns NVT run with a 1 fs timestep to let the molecular structure relax while keeping the cell dimensions fixed, followed by a 5 ns NPT run at 300 K and atmospheric pressure to allow the density and lattice parameters to settle. For the longer chains, an additional annealing step was used - the system was heated to 550 K and held for 5 ns under NPT conditions before being brought back down to 300 K to help the structure escape any kinetic traps encountered during packing. The system was considered equilibrated once both the density and total energy had plateaued into stable fluctuations with no sign of persistent drift [19].

Production runs were carried out in the NPT ensemble at 1 atm, stepping through temperatures from 300 K to 550 K in 50 K increments. At each temperature, atomic trajectories were saved at regular intervals to provide the data needed for downstream analysis. Mean-squared displacements (MSD) of polymer segments were computed from these trajectories to characterize segmental mobility and extract effective diffusion coefficients, while structural relaxation times were tracked as a function of temperature to identify the glass transition through the characteristic divergence in dynamics. Fluorine–fluorine radial distribution functions g(r) was calculated at each temperature to probe local packing and short-range structural order. Additionally, the radius of gyration (Rg) was monitored throughout each trajectory to characterize the global conformational state of the chains and assess whether equilibrium had been reached within the simulation window.

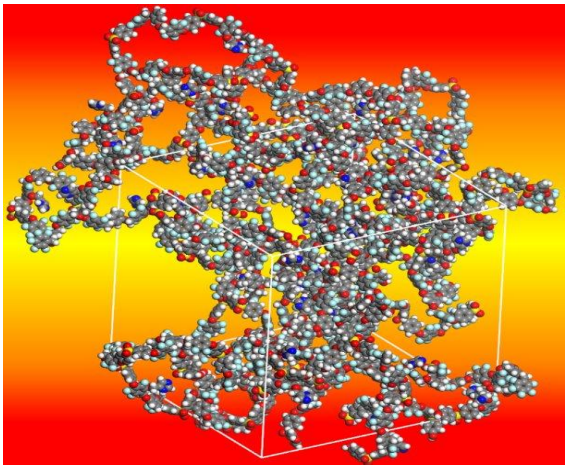

Figure 4: Optimized structure of the 8L4B-4Iz polymer in an amorphous cell following energy minimization.

2.3. Diffusion and Tg Analysis

Self-diffusion behavior in polymeric systems is characterized by computing the mean-squared displacement (MSD) of polymer segments as a function of time, where the long-time linear regime of MSD is used to extract an effective diffusion coefficient, providing a quantitative measure of segmental mobility. To reveal the strong temperature dependence of the dynamics, relaxation times or inverse diffusion coefficients are plotted as a function of temperature, which enables straightforward comparison of mobility across different architectures and conditions and allows

identification of an approximate glass transition temperature T_g from the change in slope between low-temperature glassy and high-temperature mobile regimes. Because molecular dynamics simulations are limited to nanosecond timescales, such diffusion-based T_g values are best interpreted as qualitative indicators of relative trends rather than precise experimental predictions [13-15, 19-21].

Since the glass transition is fundamentally a kinetic phenomenon associated with the drastic slowing of molecular mobility on cooling, plotting the structural relaxation time τ versus inverse temperature $1/T$ provides a more rigorous and physically meaningful approach to determining T_g than conventional volume temperature methods. As T_g is approached, τ increases by many orders of magnitude, signaling dynamic arrest; defining T_g at a characteristic relaxation time thus offers a clear, reproducible criterion directly tied to the underlying molecular dynamics. In contrast, volume temperature approaches infer T_g from changes in the slope of the thermal expansion curve and are highly sensitive to thermal history and heating/cooling rates, whereas relaxation-time-based analyses directly capture the non-Arrhenius temperature dependence of mobility and provide a more robust framework for identifying glass transition behavior in polymeric and nanocomposite systems [12-14,20,21].

2.4. Structural Analysis

To quantify local packing and short-range order, fluorine-fluorine radial distribution functions (RDFs), $g(r)$, are calculated for each system and temperature [11-13]. The first peak in $g(r)$ reflects nearest-neighbor fluorine pairs, which are typically constrained by the covalent geometry of the backbone. Second and third peaks at larger distances arise from more distant intra-chain correlations and inter-chain-like packing. The height and width of these peaks probe the degree of local structural order and dependence on, chain length, and polymer architecture.

2.5. Conformation Analysis

The radius of gyration (R_g) is employed as a global measure of the spatial extent of each polymer chain. For each trajectory and temperature, instantaneous R_g values are computed at regular intervals and used to construct a probability distribution (P) normalized such that the area under the curve (AUC) is 1, which helps in determining $P(R_g)$ that at a given radius is the R_g. Narrow distributions with a single dominant peak indicate that the chain spends most of its time in a single typical conformation, whereas broad or multimodal distributions reveal multiple coexisting conformational families. Time-dependent traces of R_g are examined to understand how the chain relaxes from its initial configuration and whether it reaches equilibrium within the simulation window.

3. RESULTS AND DISCUSSION

3.1. Relaxation Dynamics and Tg

The relaxation analysis (τ = 1/D) (Figure 5) reveals distinct temperature-dependent behavior for all three polymer architectures. For the 8-repeat unit linear chain (8L), τ increases gradually with decreasing temperature and rises sharply near 500 K, indicating an apparent T_g around this point. Above 500 K τ decreases, reflecting enhanced segmental mobility at higher temperatures.

The branched 8L4B system shows a more pronounced increase in τ at lower temperatures, with an apparent T_g near 400–450 K, which is a reasonable trend. Similarly, the imidazole-functionalized 8L4B-4Iz chain

exhibits a comparable change in slope around 400 K, though the temperature dependence of τ is slightly modified by specific interactions involving the imidazole groups.

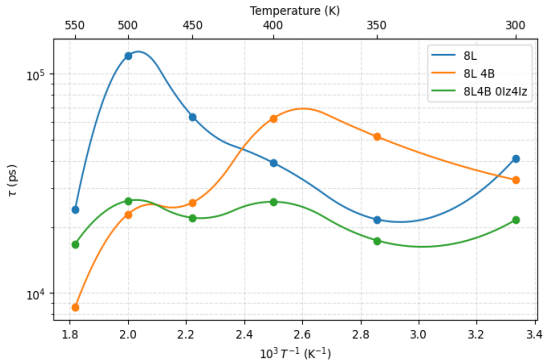

Figure 5: Relaxation time (τ) versus inverse Temperature ($1/T$) for different polymer architecture.

In contrast, the branched 8L4B system shows a moderate but noticeable increase in τ at lower temperatures, with a change in slope observed around 400–450 K, indicating a lower apparent T_g compared to 8L. Similarly, the imidazole-functionalized 8L4B-4Imz chain exhibits a smoother variation in τ, with only a subtle slope change near 400 K, suggesting that specific interactions involving the imidazole groups slightly modify the temperature dependence of relaxation without significantly shifting the transition. It should be noted that, since simulations were performed at 50 K intervals, the T_g cannot be determined precisely; finer sampling (10–25 K) would allow more accurate identification, but computational constraints limited the present study to 50 K increments.

Branching and imidazole functionalization both reduce the apparent glass transition temperature (T_g) relative to the linear reference chain. The 8L system remains comparatively rigid up to higher temperatures, whereas the branched and imidazole-functionalized architectures exhibit enhanced segmental mobility at lower temperatures. This behavior is consistent with increased structural flexibility and reduced packing efficiency introduced by branching and functional groups.

Overall, the results indicate that increasing architectural complexity lowers T_g and promotes earlier onset of dynamic motion. For membrane applications, this reduction in T_g is significant, as enhanced segmental mobility at moderate operating temperatures may facilitate proton transport.

3.2. RDF and Local Ordering

Fluorine-fluorine radial distribution functions (RDF) $g(r)$, provide insight into how local packing evolves with temperature and architecture. Across all three systems, a strong first peak shown in Figure 6 appears in the range of approximately 2.5-2.9 Å, corresponding primarily to nearest-neighbor

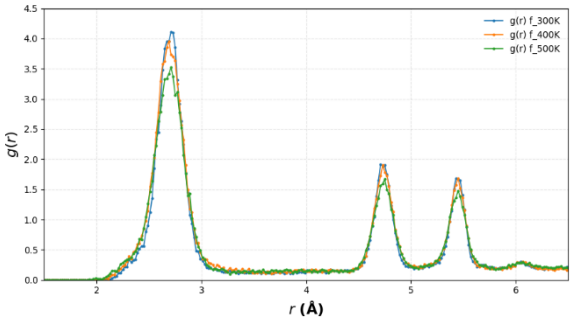

Figure 6: Radial distribution function of fluorine atoms in 8L4B-4Iz at 300K, 400K, 500K.

fluorine pairs constrained by the covalent structure of the polymer backbone. The position of this peak is essentially invariant with respect to temperature and chain architecture, as expected for distances governed by covalent bond geometry rather than thermal packing effects.

The height of this first peak, however, varies depending on how the backbone segments are arranged spatially.

Second and third peaks in $g(r)$ occur at larger distances and reflect long-range intra- and intermolecular packing correlations. The branched systems, 8L4B and 8L4B-4Iz, exhibit less pronounced and broader peaks compared to the linear 8L system.

Branching introduces topological constraints and steric hindrance that can disrupt regular packing, leading to reduced structural correlation at intermediate and longer distances. Imidazole functionalization further modifies local structure, as the presence of polar, aromatic groups introduces additional specific interactions that compete with simple backbone–backbone packing.

Temperature has a pronounced effect on the shape of $g(r)$. At 300 K, peak heights are higher and peaks are narrower, indicating a more ordered, glass-like state with limited thermal motion. As temperature increases toward 400 K and 500 K, peaks decrease in height and broaden, reflecting enhanced thermal fluctuations and a gradual transition toward a more disorder liquid-like regime. This evolution is qualitatively similar across all systems, although the magnitude of the structural changes depends on the molecular architecture.

3.3. Rg-Based Conformations

The radius of gyration (R_g) distributions reveals rich conformational behavior that complements the diffusion and RDF analyses.

Each system exhibits distinct patterns in P(R_g) - the probability distribution of the radius of gyration**,** and the time evolution of R_g.

Figure 7 shows the R_g distribution for the 8L system at temperatures from 300 K to 600 K. The R_g distribution at 300 K is broad, indicating the presence of multiple coexisting conformational families. The chain explores various compact and moderately extended configurations.

At 400 K, the distribution broadens further, consistent with increased mobility allowing the chain to sample more of its conformational landscape near the glass transition. At 500 K, however, the distribution sharpens to a narrow peak centered at a moderately extended R_g value. This suggests that once the temperature is well above T_g, the chain relaxes into a preferred extended conformation, and fluctuations around this state become relatively small over the simulation window.

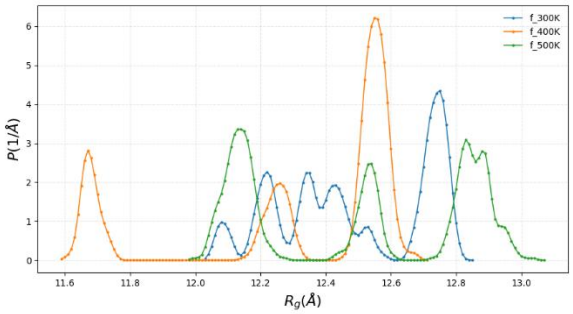

Figure 7: Radius of gyration of fluorine atoms in 8L at 300K, 400K, 500K.

The 8L4B system's R_g graph (Figure 8) shows a different pattern. Branching significantly increases the typical R_g, reflecting the larger effective volume occupied by the chain. The R_g distributions at 300, 400, and 500 K exhibit several distinct peaks, corresponding to different arrangements of the branches relative to the backbone. These topological constraints and steric effects create a variety of metastable conformational families, and the system can become trapped in specific branch orientations, especially at low temperatures. Even at higher temperatures, the branched chain retains a complex, multi-peak R_g distribution, indicating that the

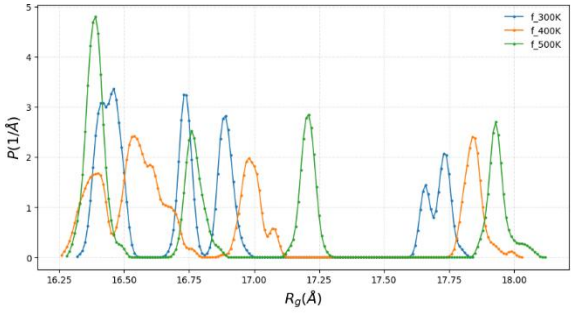

Figure 8: Radius of gyration of fluorine atoms in 8L4B at 300K, 400K, 500K.

conformational landscape remains rugged and diverse.

The imidazole-functionalized 8L4B-4Iz chain combines features of both previous systems, which can be seen in its R_g graph

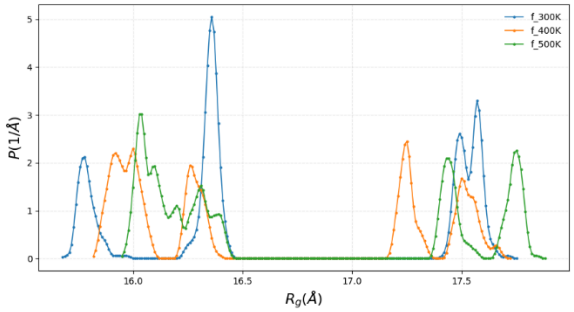

Figure 9: Radius of gyration of fluorine atoms in 8L4B-4Iz at 300K, 400K, 500K.

(Figure 9). At 300 K, the R_g distribution shows an extremely sharp dominant peak at a particular R_g, suggesting that imidazole-mediated interactions (such as π-π stacking or dipole-driven associations) stabilize a specific conformation. This "locked" state reflects strong internal interactions between imidazole groups and the rest of the chain. As temperature increases to 400 K and 500 K, the distribution broadens and secondary peaks emerge, indicating that thermal energy disrupts these specific interactions and allows the chain to explore additional conformations. These conformational behaviors have direct implications for membrane mechanical properties and the availability of free volume for proton transport.

4. CONCLUSIONS

Atomistic molecular dynamics simulations of linear and branched fluorinated polymers with and without imidazole functionalization have been used to probe the interplay between chain architecture, thermal transitions, and molecular structure in model systems for high-temperature fuel cell membranes. This study focused on three architectures: 8L, 8L4B, and 8L4B-4Iz.

Diffusion-based analysis reveals an approximate glass transition temperature near 500 K for the short linear chain (8L), while the branched (8L4B) and imidazole-functionalized (8L4B-4Iz) chains exhibit apparent T_g values closer to 400 K. This demonstrates that increased architectural complexity through branching and the incorporation of specific functional groups can significantly lower the temperature at which substantial mobility emerges.

Radial distribution functions show that local packing is strongly influenced by chain architecture. The linear 8L chain exhibits relatively strong fluorine-fluorine correlations, whereas branching in 8L4B and 8L4B-4Iz reduces long-range order while preserving short-range backbone geometry. Imidazole groups introduce additional specific local structural ordering through polar and π–π interactions. Temperature increases lead to the expected broadening and attenuation of RDF peaks across all systems, marking a gradual loss of local order as systems evolve from glassy to more liquid-like states.

Rg distributions reveal a rich set of conformational phenomena that distinguish the three architectures. The linear 8L chain transitions from multi-model glassy behavior at low temperatures to a single dominant extended state at high temperature, demonstrating thermally driven conformational ordering. The branched 8L4B chain maintains multiple conformational families across the entire studied temperature range, with topological and steric constraints preventing collapse into a single preferred state. The imidazole-functionalized 8L4B-4Iz chain exhibits-locked- conformations at low temperature due to strong imidazole-mediated interactions, such as π–π stacking and dipolar associations, which melt upon

heating to allow access to a broader conformational space.

These results provide molecular-level insights into how branching and functional groups control glass transition behavior, mobility, and structural organization in model polymer systems. The findings suggest design principles for solvent-free, high-temperature polymer electrolyte membranes for ground vehicle fuel cell applications: branching and imidazole functionalization can be used to tune glass transition temperatures and create temperature-responsive conformational behavior, while maintaining sufficient structural integrity. Future studies should examine how these architectural features influence proton transport pathways, segmental dynamics, and mechanical stability under operational conditions.

5. REFERENCES

[1] S. Mekhilef, R. Saidur, and A. Safari, "Comparative study of different fuel cell technologies," Renewable and Sustainable Energy Reviews, vol. 16, no. 1, pp. 981–989, 2012, doi: 10.1016/j.rser.2011.09.020.

[2] K. Khoiruddin, C. S. A. Nandar, S. Kawi, T. M. Lim, and I. G. Wenten, "Advanced proton exchange membranes for high-efficiency fuel cells: Material innovations and durability optimization," Energy Materials, vol. 5, art. no. 500141, 2025, doi: 10.20517/energymater.2025.62.

[3] T. Li, J. Shen, G. Chen, S. Guo, and G. Xie, "Performance comparison of proton exchange membrane fuel cells with Nafion and Aquivion perfluorosulfonic acids with different equivalent weights as the electrode binders," ACS Omega, vol. 5, no. 28, pp. 17628–17636, Jul. 2020, doi: 10.1021/acsami.2c15451.

[4] L. Friedman & P. G. Carpenter, Diffusion Velocity and Molecular Weight. I. The Limits of Validity of the Stokes–Einstein Diffusion Equation, Journal of the American Chemical Society 61, 1745–1747 (1939), doi: 10.1021/ja01876a032.

[5] O. Fernihough, M. S. Ismail, and A. El-Kharouf, "Intermediate temperature PEFC's with Nafion® 211 membrane electrolytes: An experimental and numerical study," Membranes, vol. 12, no. 4, art. no. 430, Apr. 2022, doi: 10.3390/membranes12040430.

[6] M. Saeed, M. A. El-Hameed, E. Al-Hajri, and A. Kabbani, "Water management strategies for proton exchange membrane fuel cells: A comprehensive review," Electrochem, vol. 6, no. 4, art. no. 38, Oct. 2025, doi: 10.3390/electrochem6040038.

[7] J. Yang, C. Shi, J. Li, T. Li, H. Zhang, Q. Chen, P. Wang, W. Hu, and B. Liu, "Arylether-type polybenzimidazole-based composites containing imidazole-substituted heteropolyacid salts for high-temperature proton exchange membrane fuel cells," Electrochim. Acta, vol. 504, art. no. 145007, Jan. 2025, doi: 10.1016/j.electacta.2024.145007.

[8] K. Lin, C. Wang, Z. Qiu, and Y. Yan, "Enhancement of proton conductivity performance in high temperature polymer electrolyte membrane, processed the adding of pyridobismidazole," Polymers, vol. 14, no. 7, art. no. 1283, Mar. 2022, doi: 10.3390/polym14071283.

[9] M. Muñoz, M. S. Chen, G. de Araujo Lima e Souza, T. Simunovic, V. Khokhar, P. Qian, J. Wainright, R. Savinell, A. Parnell, S. Parnell, R. C. Kilbride, T. A. Zawodzinski, and M. Dadmun, “Structured electrolytes facilitate Grotthuss-type transport for enhanced proton-coupled electron transfer reactions,” Proc. Natl. Acad. Sci. U.S.A.,

vol. 123, no. 1, Art. no. e2530367122, Jan. 2, 2026, doi:10.1073/pnas.2530367122.

[10] X. Li, H. Zhang, C. Lin, R. Tian, P. Zheng, and C. Hu, "Morphological Effect of Side Chain Length in Sulfonated Poly(arylene ether sulfone)s Polymer Electrolyte Membranes via Molecular Dynamics Simulation," Polymers, vol. 14, no. 24, Art. no. 5499, Dec. 2022, doi: 10.3390/polym14245499.

[11] F. V. Olowookere, A. Al Alshaikh, J. E. Bara, and C. H. Turner, "Effects of chain length on the structure and dynamics of polyvinyl chloride during atomistic molecular dynamics simulations," Molecular Simulation, vol. 49, no. 15, pp. 1401–1412, Jul. 2023, doi: 10.1080/08927022.2023.2234493.

[12] N. Shaari, S. H. Osman, S. K. Kamarudin, N. A. Karim, S. Basri, and A. A. Wani, "Structure–property relationships in polymer electrolyte membranes for fuel cell applications: insights from molecular dynamics simulations," Polymer Bulletin, vol. 83, art. no. 243, Feb. 2026, doi: 10.1007/s00289-026-06305-9.

[13] Allen, M. P.; Tildesley, D. J. Computer Simulation of Liquids*,* 2nd ed.; Oxford University Press: Oxford, 2017; pp 90–95.

[14] Ginzburg, V. V.; Chang, K.; Jog, P. K.; Argenton, A. B.; Rakesh, L. Correction to "Modeling the Interfacial Tension in Oil–Water–Nonionic Surfactant Mixtures Using Dissipative Particle Dynamics and Self-Consistent Field Theory" J. Phys**.** Chem. B *2013*, 117 (46), 14588.

[15] BIOVIA, Dassault Systèmes, BIOVIA Materials Studio, Release 2026, San Diego, CA, USA: Dassault Systèmes, 2024.

[16] H. Sun, "COMPASS: An ab initio force-field optimized for condensed-phase applications overview with details on alkane and benzene compounds," *Journal of Physical Chemistry B*, vol. 102, no. 38, pp. 7338–7364, 1998.

[17] S. W. Bunte and H. Sun, "Molecular modeling of energetic materials: The parameterization and validation of nitrate esters in the COMPASS force field," *Journal of Physical Chemistry B*, vol. 104, no. 11, pp. 2477–2489, 2000.

[18] C. K. Birdsall and A. B. Langdon, "Plasma Physics via Computer Simulations", McGraw-Hill Book Company, 1985, p. 56.

[19] D. N. Theodorou and U. W. Suter, "Detailed molecular structure of a vinyl polymer glass," *Macromolecules*, vol. 18, no. 7, pp. 1467–1478, 1985.

[20] K. Karakus, V. V. Ginzburg, K. Promislow, and L. Rakesh, "Modeling the glass–liquid transition in thin films: A theoretical approach using the modified Allen–Cahn model," J. Non-Cryst. Solids, vol. 672, p. 123800, Jan. 2026, doi: 10.1016/j.jnoncrysol.2025.123800.

[21] K. Karakus, V. V. Ginzburg, K. Promislow, and L. Rakesh, "Modeling the structure and relaxation in glycerol-silica nanocomposites*,"* Soft Matter*, 2025,* 21, 376–388, DOI: 10.1039/D4SM00846D & cross ref.

6. CONTACT INFORMATION

Leela Rakesh, PhD
Professor of Applied Mathematics and Polymer Fluid Dynamics
Central Michigan University
College of Science and Engineering
Department of Mathematics
Mt. Pleasant, Michigan 48859
rakes1l@cmich.edu
989-774-6524

7. ACKNOWLEDGMENT

This work was funded by the US Army: Automotive Research Center (ARC) in accordance with Cooperative Agreement W56HZV-24-2-0001 U.S. Army DEVCOM Ground Vehicle Systems Center (GVSC), Warren, MI. The authors recognize the support of Mr. Ganta and Mr. Alim without whom this work would not have been possible.

We sincerely thank the members of the Synthesis Team: Gavin Mehl from the School of Engineering and Technology, Phoenix Knipe, Milah Curry from the Department of Chemistry and Biochemistry, and Sithira Samaranayake from the Department of Physics at Central Michigan University, Mount Pleasant, MI. We are especially grateful for their meticulous work in synthesizing the polymer and characterizing its properties, which greatly contributed to refining and improving our model.

8. ACRONYMS

8L	8 repeat units
8L4B	8 units, 4 branched
8L4B-4Iz	8 units, 4 branched with imidazole
AUC	Area Under Curve
D	Diffusion Coefficient
MD	Molecular Dynamics
MSD	Mean-Squared Displacement
NVT / NPT	Simulation ensembles
P	Probability
RDF	Radial Distribution Function
τ	Relaxation Time
T_g	Glass Transition Temperature
R_g	Radius of Gyration